AN INTRODUCTION TO ION OPTICS FOR THE MASS SPECTROGRAPH

Thomas W. Burgoyne and Gary M. Hieftje*
Department of Chemistry, Indiana University, Bloomington, Indiana 47405

Abstract 241
I. Introduction 241
II. Mass Spectrograph Ion Optics 243
A. Overview, Symbols, and Coordinates 243
B. Transfer Matrix Method 243
C. Matrix Definitions for Mass Spectrograph Components 244
D. Double Focusing for a Single Reference Mass (Focal Point) 247
E. Double Focusing for Several Masses (Focal Line) 247
III. Mass Spectrograph Geometries 248
A. Bainbridge-Jordan 249
B. Mattauch-Herzog 249
C. Nier-Johnson 250
D. Hintenberger-Konig 251
E. Takeshita 251
F. Matsuda 252
G. Others 252
IV. Conclusions 255
Acknowledgments 255
References 255

A mass spectrograph is an instrument that separates and simultaneously focuses ions, along a focal plane, of different mass/charge ratios that are diverging in direction and that have a variable velocity. With these instruments and a spatially sensitive ion detector, simultaneous detection can be employed, which has been shown to improve precision and throughput (as compared to a mass spectrometer that can only detect one mass at a time). Knowing how an ion beam focuses throughout the mass spectrograph and onto the focal plane is crucial. We present here rudimentary ion optics of the mass spectrograph in a simple yet useable manner. From there, we investigate the direction and energy focal lines of some mass spectrograph geometries, using the ion optics presented. Lastly, other mass spectrograph geometries that fall outside the field of knowledge of the ion optics covered are discussed. With this review, we hope to provide an understandable and universal ion optic theory that encompasses a wide range of mass spectrographs and that is palatable to the novice as well as the expert. © 1997 John Wiley & Sons, Inc.

I. INTRODUCTION

A double-focusing mass spectrograph is "An instrument which uses both direction and velocity focusing, and therefore an ion beam initially diverging in direction and containing ions of different kinetic energies is separated into beams according to the quotient mass/charge, these beams being focused onto a photographic plate or film (Todd, 1991)." Although this definition is limited to the photographic medium, it is generally recognized to include the photographic plate's electronic counterpart, a microchannel plate (MCP) with some form of image readout. Opposed to a double-focusing mass spectrometer, a mass spectrograph can detect simultaneously more than a single mass/charge (m/z) value at any given time.

The advantages of simultaneous detection are straightforward. When one detects more than one mass at a time, less signal is wasted; therefore, sensitivity and sample throughput are improved. Simultaneous detection also

* To whom correspondence should be addressed.

Received 10 September 1996;
accepted 18 November 1996.

© 1997 by John Wiley & Sons, Inc.
CCC 0277-7037/97/040241-19

makes it easier to analyze transient samples such as those produced by flow injection, rapid chromatographic elution, microsampling, or laser ablation. Conversely, scanning requires each measured mass to be extracted from an ion source at a different point in time; thus, ratioing or normalization techniques cannot fully compensate for time-dependent fluctuations in the source. Mass scanning produces a lower signal-to-noise ratio (precision) than if the signal from all masses were measured simultaneously. This issue was emphasized by Furuta (1991), who found that the precision of lead isotope-ratio measurements taken with an inductively coupled plasma quadrupole mass spectrometer improved with an increase in the peak-jumping rate, because the effects of source and sampling drift were reduced.

Mass spectrograph development can generally be divided into three categories by the form of the array detector used (Boerboom, 1991; Birkinshaw, 1992; Staub, 1953; Wiza, 1979). As alluded to in the mass spectrograph definition, the first array detector used was the photographic plate (Thompson, 1913; Dempster, 1918; Aston, 1919; Thompson & Thompson, 1928; Aston, 1942). However, the photographic emulsion has its weaknesses. It has limited sensitivity, a low linear dynamic range (approximately 30), and the conversion of an image to numerical information is costly, nonlinear, and time-consuming. An electronic improvement to the photographic plate was called the electro-optical ion detector (EOID) (Boettger, Giffen, & Norris, 1979) and it appeared in the mid 1970s. This array detector consists of a channel electron multiplier array, phosphor screen, fiber-optic image dissector, and vidicon camera system. In other words, ions are converted to electrons, which are in turn converted to photons. The photons are converted to an electrical signal to produce a mass spectrum. The lens-camera system was an inefficient combination, and the detector did not possess the performance characteristics expected of modern systems. The linear photodiode array (PDA) or a charge-coupled device (CCD) has now replaced the vidicon camera and is the system most commonly used today.

Unfortunately, this modern array-detection system still suffers from one of the shortcomings experienced with the photographic plate; specifically, a small dynamic range. This key figure of merit is a result of the limited dynamic range of the conversion process from photons to an electrical signal; in particular, the PDA or CCD component of the array detector. An improvement in dynamic range could be experienced by varying the integration time between individual pixels in a charge injection device (CID) (Wirsz, Browne, & Blades, 1987); this development has yet to be accomplished in a mass spectrograph. Regardless of the current limited dynamic range, the prospect of improved detection limits and precision has led to the progressive development of the mass spectrograph, including the introduction of commercial instruments (Cody et al., 1994; Joel, 1996).

Lastly, some mass spectrographs contain separate Faraday cups or electron multipliers for each m/z detected. Usually, specific m/z values are chosen, such as in a carbon isotope-ratio mass spectrometer. If a large number of m/z values are desired to be detected, then this approach can be impractical and costly.

The location of the mass spectrograph focal curve or plane is imperative for instrument design, construction, and operation. A loss of instrument performance, specifically resolution, will occur if the array detector and focal region are not aligned. Second, during the eventual optimization of the detector location in a mass spectrograph, the difference between the theoretical and actual array detector placement can be used as an indicator of possible instrument problems.

From the first mass spectrographs of Thomson, Dempster, and Aston (Thompson, 1913; Dempster, 1918; Aston, 1919; Thompson & Thompson, 1928; Aston, 1942), many additional mass spectrographs have been designed and built (Boettger, Giffen, & Norris, 1979; Cody et al., 1994; Mattauch & Herzog, 1934; Dempster, 1935; Bainbridge & Jordan, 1936; Mattauch, 1936; Herzog & Hauk, 1938; Jordan, 1941; Mattauch, 1953; Ogata & Matsuda, 1953; U.S. National Bureau of Standards, 1953; Ewald, Sauermann, & Liebl, 1959; Hintenberger & Konig, 1959; Spencer & Reber, 1963; Hedin & Nier, 1966; Euge, 1967; Mai & Wagner, 1967; Takishita, 1967; Hayes, 1969; Euge et al., 1971; Nier & Hayden, 1971; Alexeff, 1973; Bakker, 1973; Carrico, Johnson, & Somer, 1973; Nier et al., 1973; Oron & Paiss, 1973; Dreyer et al., 1974; Giffen, Boettger, & Norris, 1974; Beynon, Jones, & Cooks, 1975; Tuithof, Boerboom, & Meuzelaar, 1975; Berthod & Stefani, 1976; Oron, 1976; Tuithof et al., 1976; Enge & Horn, 1977; Mauersberger, 1977; Moore, 1977; Salomaa & Enge, 1977; Taylor & Gorton, 1977; Alexiff, 1978; Forrester, Perel, & Mahoney, 1978; Tsoupas et al., 1978; von Zahn & Mauersberger, 1978; Enge, 1979; Mauersberger & Finstad, 1979; Waegli, 1979; Donohue, Carter, & Mamantov, 1980; Louter et al., 1980; Nowak et al., 1980; Wollnik, 1980; Hedfjall & Ryhage, 1981; Louter & Buijserd, 1983; Louter, Buijserd, & Boerboom, 1983; Chamel & Eloy, 1984; Coplan, Moore, & Hoffman, 1984; Murphy & Mauersberger, 1985; Nier & Schlutter, 1985; Cottrell & Evans, 1987; Cottrell & Evans, 1987; Ghielmetti & Young, 1987; Murphy & Mauersberger, 1987; Young et al., 1987; Boerboom & Meuzelar, 1988; Leclercq & Cramers, 1988; Matsuda & Wollnik, 1988; Bradshaw, Hall, & Sanderson, 1989; Hill et al., 1989; Ishihara & Kammei, 1989; Leclercq et al., 1989; Matsuda, 1989; Matsuda & Wollnik, 1989; Matsuo, Sakurai, & Derrick, 1989; Burlingame et al., 1990; Gross, 1990; Matsuo, Sakurai & Ishihara, 1990; Sinha, 1990; Gross et al., 1991; Hill, Biller, &

Biemann, 1991; Mantus, Valaskovic, & Morrison, 1991; Sinha & Gutnikov, 1991; Li, Duhr, & Wollnik, 1992; Sinha & Gutnikov, 1992; Sinha & Tomassian, 1992; Walder & Freeman, 1992; Bratschi et al., 1993; Ghielmetti et al., 1993; Hirahara & Mukai, 1993; Matsuo & Ishihara, 1993; Walder et al., 1993; Walder, Platzner, & Freeman, 1993; Rytz, Kopp, & Eberhardt, 1994; Wurz et al., 1995; Cromwell & Arrowsmith, 1996; Burgoyne, Hieftje, & Hites, 1996). Yet, despite the development of these instruments, no single source in the literature exists to provide a simple, concise, and useful means of describing the ion optics and double-focusing focal planes of these types of instruments. Thus, the goals of the present review are: (a) to present rudimentary ion optics of the mass spectrograph in a simple yet useable manner, and (b) to investigate the direction and energy focal lines of some mass spectrograph geometries, using the ion optics presented.

II. MASS SPECTROGRAPH ION OPTICS

A. Overview, Symbols, and Coordinates

We will limit our discussion of ion optics to field-free regions, electrostatic quadrupoles, electric sectors (ESA or electrostatic analyzer), and magnetic sectors with an oblique entrance and exit angle. Other mass spectrograph components such as Wien filters (Aberth & Wollnik, 1990), magnetic quadrupoles (Courant, Livingston, & Snyder, 1952), and fringing fields (Wollnik, 1965; Wollnik & Ewald, 1965) will not be discussed. Second and higher-order matrices will be ignored (Penner, 1961; Brown, Belbeach, & Bounin, 1964; Wollnik, 1967; Wollnik, 1967; Enge, 1967; Matsuda, 1983). In general, higher-order focusing occurs at one point on the double-focusing line and does little to improve simultaneous detection in a mass spectrograph. Typically, this point is employed for a point detector such as a Faraday cup or an electron multiplier. Note that for more precise trajectory determination, higher order calculations are usually required as well as the influence of fringing fields. Topics such as those are advanced, and do not fit within the scope of this review.

Table I is a glossary of symbols, and Fig. 1 defines the x, y, and z coordinate system that is used throughout the text. All calculations start with an ion beam formed from a slit (the object) with a known mass (m_o, in Daltons), energy (E, in eV), width (x, in meters), and angle of divergence (α, in radians). There are several excellent sources on the general subject of ion optics and mass spectrometry, which we suggest that the reader consult for further introductory information (U.S. National Bureau of Standards, 1953; Enge, 1967; Moore, Davis, & Coplan, 1983; Bainbridge, 1953; McDowell, 1963; Dahl, 1973; Wollnik, 1987).

B. Transfer Matrix Method

The image along the focal plane of the mass spectrograph will be determined using the method of transfer matrices (Wollnik, 1987; Banford, 1966; Ioanoviciu, 1989). Using transfer matrices, one can calculate the location of a reference ion given the initial ion conditions and the specific ion-optic geometry of the mass spectrometer. With this approach, a mass spectrograph is divided into segments, with each segment represented by a matrix. For example, a general mass spectrograph is shown in Fig. 2 and is divided into seven segments (starting from the image, through the sector elements, to the object or image-defining slit): a drift length or field-free region (matrix [DL3]); a magnetic sector with oblique entrance and exit angles (matrices [OEM2], [MAG], and [OEM1]); another drift length (matrix [DL2]); an electric sector (matrix [ESA]); and, lastly, a drift length (matrix [DL1]). By multiplying these seven transfer matrices, an overall matrix is generated, from which one can determine the ion-beam characteristics at the focal point, given some specified initial ion-beam characteristics:

$$[\text{FINALMATRIX}] = [\text{DL3}][\text{OEM2}][\text{MAG}][\text{OEM1}][\text{DL2}][\text{ESA}][\text{DL1}]. \quad (1)$$

A general, first-order matrix is shown below:

$$\begin{bmatrix} x_7 \\ a_7 \\ \partial E \\ \partial M \end{bmatrix} = \begin{bmatrix} x_7|x_1 & x_7|a_1 & x_7|\partial E & x_7|\partial M \\ a_7|x_1 & a_7|a_1 & a_7|\partial E & a_7|\partial M \\ 0 & 0 & 1 & 0 \\ 0 & 0 & 0 & 1 \end{bmatrix} \begin{bmatrix} x_1 \\ a_1 \\ \partial E \\ \partial M \end{bmatrix}, \quad (2)$$

where x is the beam width (meters), a is the angle of divergence (radians, $a \approx \tan \alpha$), ∂E is the energy dispersion, and ∂M is the mass dispersion. A similar matrix exists for the y-direction, but calculations here will be limited to those pertaining to the x-direction. The subscript 1 on x and a represents the initial ion-beam condition, and the 7 subscript represents the beam characteristics after the seventh transfer matrix (in this case, at the focal plane). We are using this matrix to "transfer" beam conditions from one location of a mass spectrograph to another. Each element in the 4×4 matrix provides some information. For example, $x_7|x_1$ represents the final image width x_7 solely as a function of the initial width x_1. This ratio is commonly called the magnification. For convenience, the

TABLE I. Glossary of symbols.

α	angle of divergence (see Fig. 1)	m_o	reference mass
a	angle of divergence, $a \approx \tan \alpha$	R	resolution
α_o	initial angle of divergence (see Fig. 1)	R_e	electric sector radius
a_o	initial angle of divergence, $a_o \approx \tan \alpha_o$	R_m	magnetic sector radius for mass m_o
B	magnetic field strength	R'_m	magnetic sector radius for mass m
∂M	mass dispersion	R_q	quadrupole rod radius
∂E	energy dispersion	S	slit width
d	distance between + and − ESA plates	θ	angle difference between Φ_M and Φ'_M
E	ion beam energy	x	image width
ϵ'	magnetic sector entrance angle	x_o	initial image width
ϵ''	magnetic sector exit angle	X	x-coordinate for location of focal point of mass m
Φ_E	electric sector angle		
Φ_M	magnetic sector angle for mass m_o	X_o	x-coordinate for ion beam of mass m entering the magnetic sector
Φ'_M	magnetic sector angle for mass m		
γ	relative mass difference ($m = m_o(1 + \gamma)$)	X'	x-coordinate for ion beam of mass m leaving the magnetic sector, $X' = 0$ for mass m_o
κ	angle between focal line and normal to the optic axis (Fig. 2)		
L_α	length from the magnetic sector to the direction-focusing point	$\pm V_{ESA}$	voltage applied to the ESA
		$\pm V_q$	voltage applied to quadrupole rods
L_E	length from the magnetic sector to the energy-focusing point	z	number of charges
		Z	x-coordinate for location of focal point of mass m
L_q	length of electrostatic quadrupole		
G	field radius of an electrostatic quadrupole	Z_o	z-coordinate for ion beam of mass m entering the magnetic sector
I_{FL}	image width along the focal line		
κ	angle between focal line and normal to the optic axis	Z'	z-coordinate for ion beam of mass m leaving the magnetic sector, $Z' = 0$ for mass m_o
K	value defined for electrostatic quadrupole		
Δm	difference between high and low mass		

subscripts are usually dropped (i.e., $x_7|x_1 = x|x$) and we will use the same convention here.

The matrix elements in Eq. (2) can be used to determine, for example, the image width at the focal plane (I_{FP}):

$$I_{FP} = (S(x|x) + a_o(x|a)) \times \cos(\kappa), \tag{3}$$

where S is the slit width in meters, a_o is the initial angle of divergence, and κ is the angle between the focal line and normal to the optic axis. Also, resolution (R) can be calculated from the matrix elements (given no exit slit):

$$R = \frac{x|\partial M}{I_{FP}}. \tag{4}$$

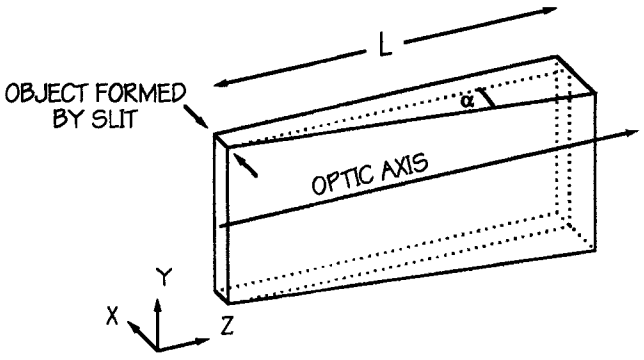

FIGURE 1. Diagram of ion beam in field-free region of width x_o and angular divergence α_o.

C. Matrix Definitions for Mass Spectrograph Components

We will now discuss the individual matrices for the components in a mass spectrograph. We simply present the matrices themselves and recommend the reader to Wollnik's book (1987) on the subject for the derivation. Additionally, programs that calculate transfer matrices of sector-field mass spectrometer systems, such as GIOS (Wollnik, Brezina, & Wendel, 1984; Wollnik, Brezina, & Berz,

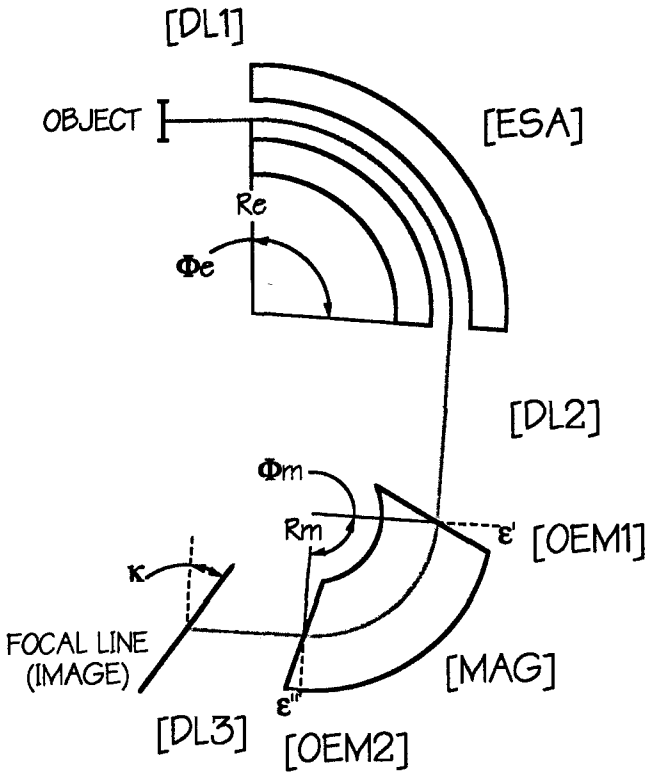

FIGURE 2. Example mass spectrograph. Bracketed notation indicates matrix type. [DL1] = matrix for first drift length, [ESA] = matrix for electric sector, [DL2] = matrix for second drift length, [OEM1] = matrix for oblique entrance angle into the magnetic sector, [MAG] = matrix for magnetic sector, [OEM2] = matrix for oblique exit angle into the magnetic sector, and [DL3] = matrix for third drift length.

1987), TRIOS (Matsuo et al., 1976), and ISIOS (Yavor, 1993) have been developed.

Drift Length. A drift length is a field-free region of length L_{dl}, where no acceleration, deceleration, or focusing of the ion beam occurs (Fig. 1). The matrix elements for this mass spectrograph component are:

$$x|x = 1,\ x|a = L_{dl},\ x|\partial E = 0,\ x|\partial M = 0, \tag{5}$$

$$a|x = 0,\ a|a = 1,\ a|\partial E = 0,\ a|\partial M = 0. \tag{6}$$

Electrostatic Quadrupole. An electrostatic quadrupole is composed of four rods that surround the optic axis. For focusing in the x-direction, positive DC potentials ($+V_q$) are applied to the poles along the x-axis and negative DC potentials ($-V_q$, for defocusing) along the y-direction (as in Fig. 3). A second quadrupole (together called a quadrupole doublet) may follow for focusing along the y-direction and subsequent defocusing along the x-direction. Although the voltage magnitudes are usually identical, in practice small voltage differences can be applied to the rods to change the beam direction. Electrostatic quadrupoles can, therefore, steer and focus the ion beam. When circular rods are used, electrostatic fields are closest to ideal when the field radius (G) is 1.148 R_q, the radius of the rods (Denison, 1971; Dawson, 1995). Before giving the matrix elements for an electrostatic quadrupole, we shall first define the quantity K:

$$K = \sqrt{\frac{abs(V_q)}{G^2 E}}, \tag{7}$$

where V_q and G are defined above and E is the ion-beam energy. The matrix elements for an electrostatic quadrupole of length L_q (in meters) are:

$$x|x = \cos(L_q K), \tag{8}$$

$$x|a = \frac{1}{K}\sin(L_q K), \tag{9}$$

$$x|\partial E = x|\partial M = 0, \tag{10}$$

$$a|x = -K^2 \sin(L_q K), \tag{11}$$

$$a|a = \cos(L_q K), \tag{12}$$

$$a|\partial E = a|\partial M = 0. \tag{13}$$

If V_q is negative (defocusing along the x-direction), then the hyperbolic cosine replaces the cosine functions and the hyperbolic sine replaces the sine functions above. Note that the mass and energy dispersions are zero, indicating that these elements are simply used for focusing and not for mass or energy dispersion.

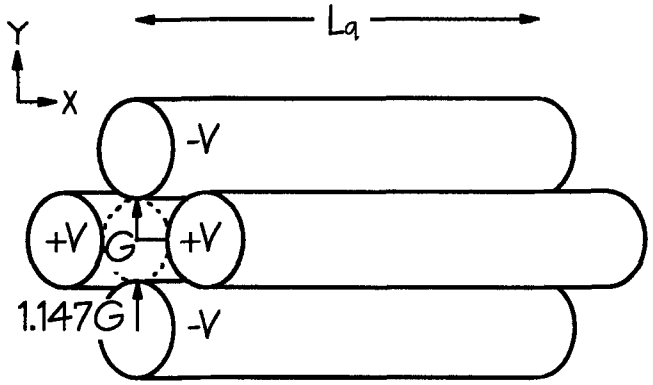

FIGURE 3. Diagram of an electrostatic quadrupole.

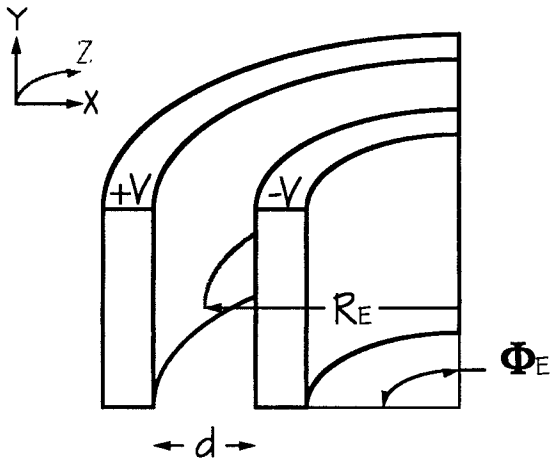

FIGURE 4. Diagram of an electric sector (ESA).

Electric Sector. An electric sector or ESA (Fig. 4) is composed of a section (angle Φ_e) of two circular plates with a center line of curvature equal to radius R_e. The voltage on the two plates is determined from:

$$\pm V_{ESA} = \frac{d \times E}{R_e}, \tag{14}$$

where d is the distance between the two plates in meters and E is the ion-beam energy. As with the electrostatic quadrupole, the theoretical potentials on the plates are equal but opposite. In practice, small voltage differences can be used to alter the beam direction. The matrix elements for an electric sector are:

$$x|x = \cos(\sqrt{2}\Phi_e), \tag{15}$$

$$x|a = \frac{R_e}{\sqrt{2}} \sin(\sqrt{2}\Phi_e), \tag{16}$$

$$x|\partial E = \frac{R_e}{2}(1 - \cos(\sqrt{2}\Phi_e)), \tag{17}$$

$$x|\partial M = 0, \tag{18}$$

$$a|x = -\frac{\sqrt{2}}{R_e} \sin(\sqrt{2}\Phi_e), \tag{19}$$

$$a|a = \cos(\sqrt{2}\Phi_e), \tag{20}$$

$$a|\partial E = \frac{1}{\sqrt{2}} \sin(\sqrt{2}\Phi_e), \tag{21}$$

$$a|\partial M = 0. \tag{22}$$

Note that the mass dispersion is zero, indicating that the electric sector functions independently of mass.

Sense Matrix. When combining an electric and a magnetic sector, some geometries change the bending direction (this change does not occur in our example mass spectrograph in Fig. 2). This change in beam direction is accommodated by incorporating a sense matrix before and after the matrix for electric sector (i.e., [SENSE][ESA][-SENSE]) (Matsuo & Ishihara, 1993); the elements of this matrix are:

$$x|x = -1, \quad x|a = 0, \quad x|\partial E = 0, \quad x|\partial M = 0, \tag{23}$$

$$a|x = 0, \quad a|a = -1, \quad a|\partial E = 0, \quad a|\partial M = 0. \tag{24}$$

Magnetic Sector. A magnetic sector consists of a north and a south magnetic pole separated by a narrow distance (no greater than about 1 cm) (Fig. 5). This sector is described by an angle and radius of deflection for the reference ion, Φ_m and R_m (in radians and meters), respectively. The radius of deflection for a reference mass (m_o) is described by the well-known equation:

$$\frac{m_o}{z} = 4.8242657 \times 10^7 \frac{R_m^2 B^2}{E}, \tag{25}$$

where z is the number of charges on the ion ($1, 2 \cdots$), B is the magnetic field strength in Tesla, E is the ion beam energy in eV, and R_m and m_o are as described above. The constant formulates for the equation in the above units. The matrix elements for a magnetic sector are:

$$x|x = \cos(\Phi_m), \tag{26}$$

$$x|a = R_m \sin(\Phi_m), \tag{27}$$

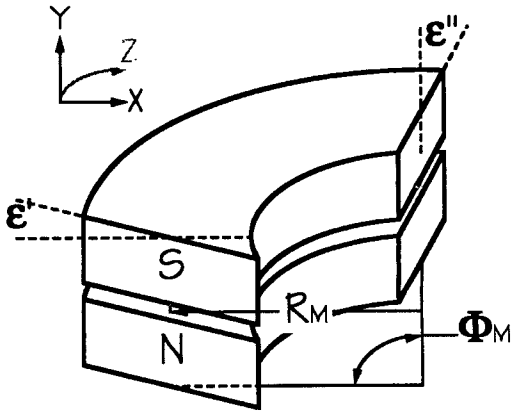

FIGURE 5. Diagram of a magnetic sector with oblique entrance and exit angles.

$$x|\partial E = \frac{R_m}{2}(1 - \cos(\Phi_m)), \quad (28)$$

$$x|\partial M = \frac{R_m}{2}(1 - \cos(\Phi_m)), \quad (29)$$

$$a|x = -\frac{1}{R_m}\sin(\Phi_m), \quad (30)$$

$$a|a = \cos(\Phi_m), \quad (31)$$

$$a|\partial E = \frac{1}{2}\sin(\Phi_m), \quad (32)$$

$$a|\partial M = \frac{1}{2}\sin(\Phi_m). \quad (33)$$

Oblique Entrance and Exit of Magnetic Sector. The above matrix is solely for an ion beam that enters and exits the magnetic sector in a direction normal to the pole face. Oftentimes, changing the angle of the pole face will improve the focusing capabilities of a mass spectrograph. This angle is noted as ε with a prime superscript (ε') to indicate the entrance of the magnet and a double prime (ε'') to indicate the exit of the magnet (see Figs. 2 and 5). ε is positive if the normal to the pole face is farther from the origin of R_m than the optic axis; ε is negative if it is closer to the origin of R_m. A positive entrance angle exhibits a focusing action in the y-direction, as noted earlier (Herzog, 1950). Sometimes, the pole face is curved to improve second-order focusing; however, this embellishment will not be discussed any further here. The matrix elements for an oblique entrance or exit of the magnetic sector are:

$$x|x = 1, \quad x|a = 0, \quad x|\partial E = 0, \quad x|\partial M = 0, \quad (34)$$

$$a|x = \frac{\tan(\varepsilon)}{R_m}, \; a|a = 1, \quad a|\partial E = 0, \quad a|\partial M = 0, \quad (35)$$

where ε can be either ε' or ε''.

D. Double Focusing for a Single Reference Mass (Focal Point)

From the matrices, we can determine the focal point (the condition where the direction- and energy-focusing points coincide) of our mass spectrograph for a reference mass m_o. First, let us solve the matrix [M] for our example mass spectrograph (Fig. 2) from the oblique exit angle of the magnet to the first drift length:

$$[\mathrm{M}] = [\mathrm{OEM2}][\mathrm{MAG}][\mathrm{OEM1}][\mathrm{DL2}][\mathrm{ESA}][\mathrm{DL1}]. \quad (36)$$

We will identify each element in this matrix [M] by the subscript M (i.e., $(x|x)_M$, $(x|a)_M$, etc.). The final matrix for this mass spectrograph is calculated from [MATRIX] = [DL3][M] or:

$$[\mathrm{MATRIX}] = \begin{bmatrix} 1 & L & 0 & 0 \\ 0 & 1 & 0 & 0 \\ 0 & 0 & 1 & 0 \\ 0 & 0 & 0 & 1 \end{bmatrix} \times \begin{bmatrix} (x|x)_M & (x|a)_M & (x|\partial E)_M & (x|\partial M)_M \\ (a|x)_M & (a|a)_M & (a|\partial E)_M & (a|\partial M)_M \\ 0 & 0 & 1 & 0 \\ 0 & 0 & 0 & 1 \end{bmatrix}, \quad (37)$$

where the third drift length consists of length, L. Multiplying the two matrices produces:

$$[\mathrm{MATRIX}] = \begin{bmatrix} (x|x)_M + L(a|x)_M & (x|a)_M + L(a|a)_M & (x|\partial E)_M + L(a|\partial E)_M & (x|\partial M)_M + L(a|\partial M)_M \\ (a|x)_M & (a|a)_M & (a|\partial E)_M & (a|\partial M)_M \\ 0 & 0 & 1 & 0 \\ 0 & 0 & 0 & 1 \end{bmatrix}. \quad (38)$$

For direction focusing, the matrix element $x|a = 0$, or from Eq. (38):

$$L_\alpha = -\frac{(x|a)_M}{(a|a)_M}. \quad (39)$$

Likewise, for energy focusing, the matrix element $x|\partial E = 0$. Also, from Eq. 38:

$$L_E = -\frac{(x|\partial E)_M}{(a|\partial E)_M}. \quad (40)$$

Therefore, by solving the matrix up to the final drift length for any mass spectrograph, one can determine the location of the direction- and energy-focusing points. A double-focusing mass spectrometer has the condition $L_\alpha = L_E$.

E. Double Focusing for Several Masses (Focal Line)

Determining the focal points for several masses in a mass spectrograph is identical to the method described above except that, from Eq. (25), a mass different from the refer-

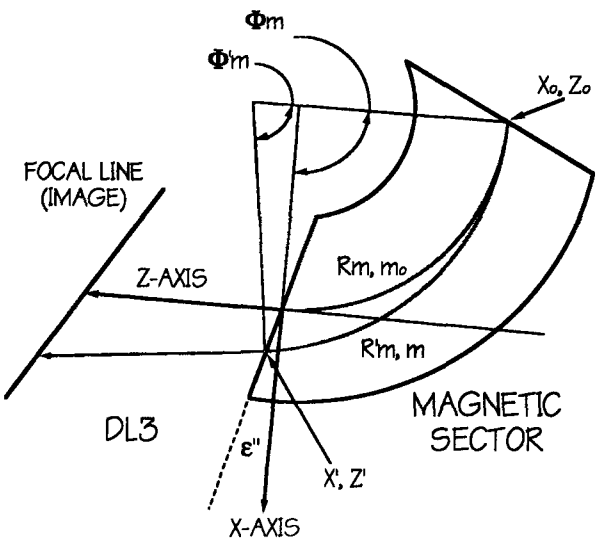

FIGURE 6. Diagram of a magnetic sector with X, Z coordinate notation.

ence mass results in a different radius (we indicate the radius in the magnetic sector that is not for the reference mass by means of a superscript prime, R'_m). A coordinate system is required to locate where the ion will exit the magnet relative to the reference mass, m_o. A coordinate system has been developed by Matsuo et al. (1989), and we present the pertinent information here.

Figure 6 is a detailed drawing of the magnetic sector of our example mass spectrograph from Fig. 2. From Eq. (25), and knowing the mass difference between m and m_o (where $m = m_o(1 + \gamma)$), one can determine the radius difference:

$$\sqrt{\frac{m_o}{m}} = \frac{R_m}{R'_m} = \sqrt{1 + \gamma}\,. \tag{41}$$

We can determine the angle of deflection of $R'_m(\Phi'_m)$ from:

$$\Phi'_m = \Phi_m - \varepsilon'' + \sin^{-1}\left[(\sin(\Phi_m - \varepsilon'') + \sin(\varepsilon'')\frac{R_m}{R'_m} - \sin(\Phi_m - \varepsilon'')\right]. \tag{42}$$

The angular difference between Φ_m and Φ'_m, θ, is:

$$\theta = \varepsilon'' - \sin^{-1}\left[(\sin(\Phi_m - \varepsilon'') + \sin(\varepsilon'')\frac{R_m}{R'_m} - \sin(\Phi_m - \varepsilon'')\right]. \tag{43}$$

Lastly, we need to know the where mass m leaves the magnetic sector. Here, we use the X', Z' coordinates to denote where an ion of mass m exits the magnetic sector (relative to X_o and Z_o, see Fig. 6):

$$X' = R'_m[\cos(\Phi'_m - \Phi_m) - \cos(\Phi_m)] - R_m(1 - \cos(\Phi_m)) \tag{44}$$

$$Z' = R'_m[\sin(\Phi'_m - \Phi_m) + \sin(\Phi_m)] - R_m \sin(\Phi_m). \tag{45}$$

From the above equations, we can locate the direction and energy focal points for a given mass from:

$$X = X' + L_\alpha \sin(\theta) \tag{46}$$

$$Z = Z' + L_\alpha \cos(\theta) \tag{47}$$

$$X = X' + L_E \sin(\theta) \tag{48}$$

$$Z = Z' + L_E \cos(\theta). \tag{49}$$

Again, L_α and L_E are determined by first specifying the mass difference (γ) that the mass spectrograph will analyze. The new radius and angle of deflection (R'_m and Φ'_m) are determined from Eqs. (41) and (42). By calculating the matrix up to the last drift length, as in Eq. (36), the direction and energy drift lengths (L_α and L_E) can be determined from Eqs. (39) and (40) and placed in an X, Z coordinate system [from Eqs. (46)–(49)], where the X, Z origin is where the ion of reference mass m_o leaves the magnetic sector (see Fig. 6).

This calculation is involved and can be overwhelming if attempted without the aid of a computer. Therefore, all of the above equations were formatted in Pascal and run under CodeWarrior (Metrowerks, Austin, TX) with a Macintosh Powerbook 5300c (Burgoyne, 1996). Other math programs, such as Mathcad (MathSoft, Cambridge, MA) or Mathmatica (Wolfram Research, Champaign, IL), could also be used to solve the equations presented above. The above-mentioned Pascal program was used to generate all of the focal line plots of the mass spectrographs below.

For our example mass spectrograph (Fig. 2), the focal line is given in Fig. 7. All values are in meters. The direction-focusing line is a solid black line and the energy-focusing line is the gray dashed line (for this and all subsequent plots). Notice that at $X = 0$, $Z = 0.947$ m, which is the drift length for the reference mass, m_o. Fitting a straight line to both focal lines, the angle (κ) between the normal to the optic axis and the focal line is determined by calculating the tangent of the slope.

III. MASS SPECTROGRAPH GEOMETRIES

What follows is a brief discussion of a few selected mass spectrograph geometries. In addition, the focal line for

TABLE II. Matrix elements for some selected mass spectrograph geometries.

Geometry/element	$x\|x$	$x\|a$	$x\|\partial E$	$x\|\partial M$	$a\|x$	$a\|a$	$a\|\partial E$	$a\|\partial M$
Bainbridge–Jordan	1.000	2.092×10^{-4}	-2.55×10^{-5}	2.540×10^{-1}	3.407	1.001	-4.327×10^{-1}	4.330×10^{-1}
Bainbridge–Jordan[a]	3.341×10^{-1}	6.2×10^{-6}	1.90×10^{-5}	8.488×10^{-2}	5.666	2.993	−1.295	1.454×10^{-1}
Mattauch–Herzog	-6.482×10^{-1}	6.0×10^{-7}	0.000	9.075×10^{-2}	4.792	−1.543	1.442	-1.0×10^{-7}
Nier–Johnson	6.786×10^{-1}	7.98×10^{-5}	-1.278×10^{-5}	1.279×10^{-1}	14.483	1.475	1.470	0.433
Nier–Johnson[a]	2.586×10^{-1}	-8.0×10^{-6}	-1.04×10^{-5}	4.878×10^{-2}	32.654	3.867	−3.851	1.351×10^{-1}
Hintenberger–Konig	8.957×10^{-1}	-4.678×10^{-4}	-6.680×10^{-4}	8.214×10^{-1}	-7.402×10^{-1}	1.117	1.363	0.000
Takeshita	-5.620×10^{-1}	1.4330×10^{-3}	1.673×10^{-4}	1.000	3.099×10^{-1}	−1.780	-7.069×10^{-1}	0.000
Matsuo–Type	4.618×10^{-1}	1.884×10^{-2}	-1.704×10^{-2}	7.769×10^{-1}	2.233	2.257	−2.039	4.679×10^{-1}

[a] Indicates modified geometry from original design. See text for details.

each of these mass spectrographs has been calculated as explained above for $\gamma = -0.5$ to $+0.5$. The Initial ion-beam energy was assumed to be 5000 eV with an energy distribution of 5 eV. Also, the matrix elements for each of the mass spectrographs are presented, using the geometry values listed in the corresponding figures (see Table II).

A. Bainbridge–Jordan

From Fig. 8, the Bainbridge–Jordan mass spectrograph geometry consists of a $\pi/\sqrt{2}$ ESA without an initial drift length.[18] From Hughes and Rojansky (1929), it is known that an ion beam with a slight divergence in an ESA will cross at every $\pi/\sqrt{2}$ (unlike in a magnetic sector, where an ion beam will cross at every π). Therefore, angular divergence at the source will result in a focus at the end of the ESA in this instrument. The magnetic sector focuses the beam using Barber's Rule (the object, center of deflection, and image lie along a straight line) (Barber, 1933). Figure 9 represents the focal line of this instrument, and, as is evident, it does not do a very good job of focusing all of the ions.

Oftentimes, simply changing the exit angle of the magnetic sector will improve the focusing properties of the mass spectrograph. Figure 10(A) is the summed distance between the direction- and energy-focusing lines for a variety of exit magnetic-sector angles for the Bainbridge–Jordan mass spectrograph. The smallest distance between the lines occurs at an angle of −49° (Herzog & Hauk, 1938), and this change in the exit angle improves the focal line considerably [Fig. 10(B)]. Note also that the last drift length before the focal line has changed from 0.44–0.15 M.

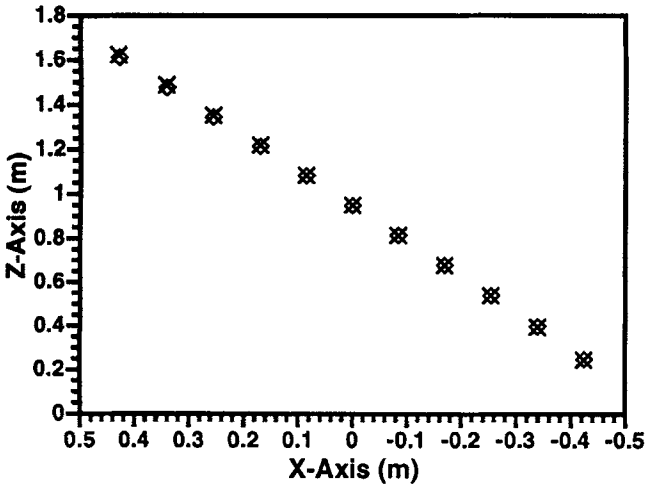

FIGURE 7. Focal line of the example mass spectrograph (see Fig. 2). × = direction-focusing point and ◇ = energy-focusing point. A fitted direction-focusing line results in $\kappa = 58.1°$. A fitted energy-focusing line results in $\kappa = 57.9°$.

B. Mattauch–Herzog

J. Mattauch and R. Herzog noted that a mass spectrograph that did not have a focal point between the electric and magnetic sector (the ion beam is collimated as it enters the magnetic sector) could provide double focusing independent of the magnetic-sector radius. This lack of focal point meant double focusing for all masses. For this geometry, second-order angular-aberration focusing occurs at $R_e/R_m = 1.683$. For more information on this geometry, see Mattauch's manuscripts (Mattauch & Herzog, 1934; Mattauch, 1936; Mattauch, 1953). A beam is collimated leaving the ESA by setting the object at the length (DL1):

$$\mathrm{DL1} = \frac{R_e}{\sqrt{2}} \cot(\sqrt{2}\Phi_e). \tag{50}$$

After the second drift length (which is after the ESA), the

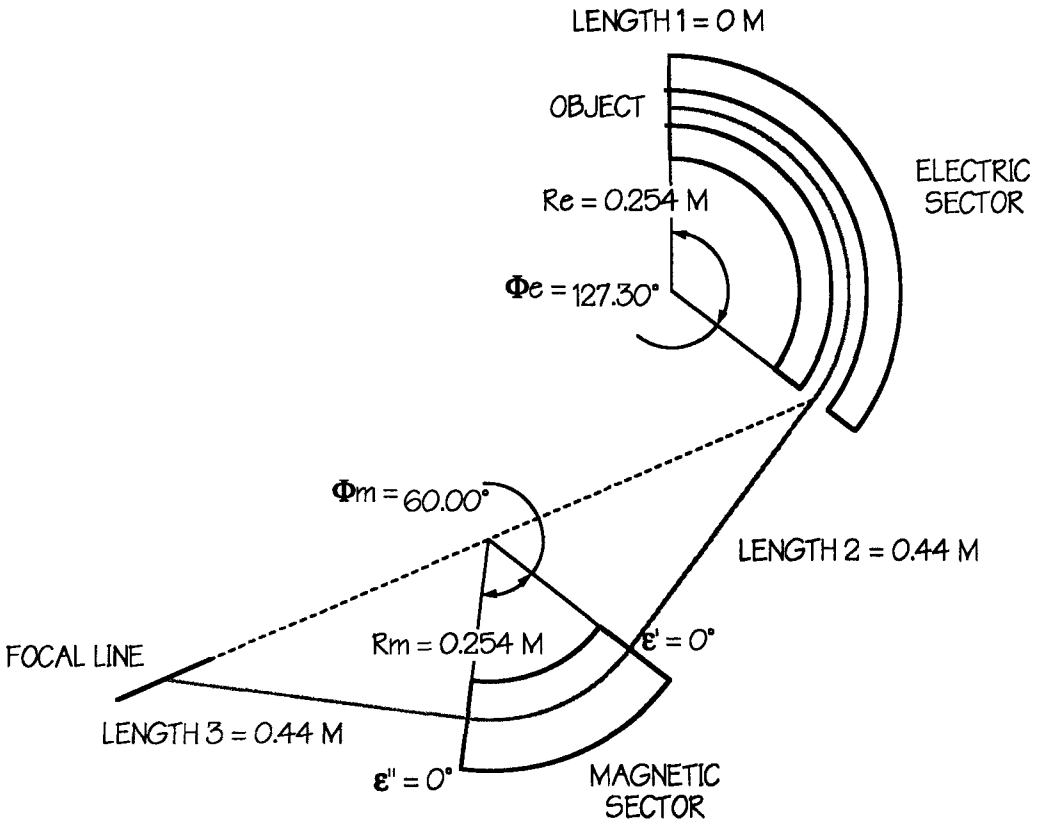

FIGURE 8. Diagram of the Bainbridge–Jordan mass spectrograph geometry.

collimated ion beam enters normal to the magnetic sector and undergoes $\pi/2$ of deflection with an oblique exit angle of $-\pi/4$ (Fig. 11). With this geometry, the ion beam changes direction and, for this calculation, the sense matrix is needed, as indicated earlier. The direction and energy focal lines are located at the end of the magnetic sector and overlap well (Fig. 12).

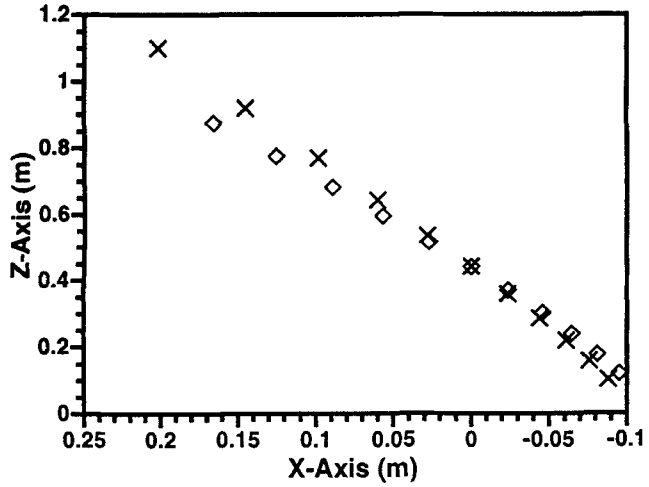

FIGURE 9. Focal line of the Bainbridge–Jordan mass spectrograph. × = direction-focusing point and ◇ = energy-focusing point. A fitted direction-focusing line results in $\kappa = 73.7°$. A fitted energy-focusing line results in $\kappa = 70.8°$.

C. Nier–Johnson

The Nier–Johnson geometry (Fig. 13) is generally considered as a focal-point mass spectrometer (Nier & Roberts, 1951; Johnson & A.O., 1953) and not as a mass spectrograph. However, the angle and energy focal lines match over a limited mass range, enabling this geometry to be used as a mass spectrograph (Hill et al., 1989). The original purpose of the Nier–Johnson design was to eliminate second-order angular aberrations (that is, to improve second-order direction focusing). The focal lines are presented in Fig. 14.

As with the Bainbridge–Jordan geometry (Fig. 8), altering the exit magnetic sector angle improves the focal line of this geometry. The best overlap of the two focal lines occurs at −50° (Matsuo & Isuihara, 1993), an oblique exit angle that also shortens the final drift length [Figs. 15(A) and (B), respectively].

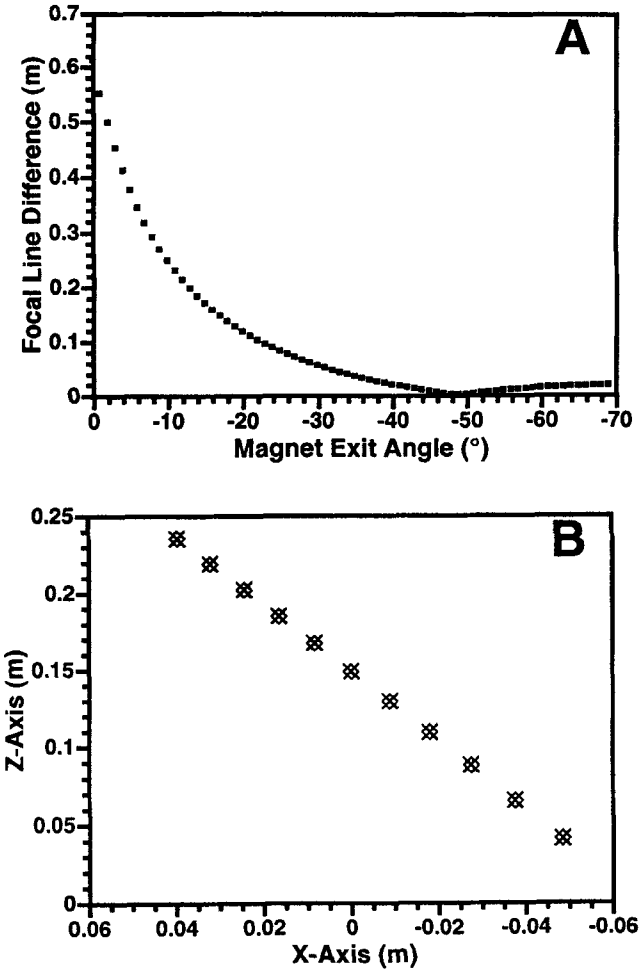

FIGURE 10. (A) Difference in direction and energy focal lines as a function of oblique exit angle of the magnetic sector (ε''). The smallest distance between focal lines is $\varepsilon'' = -49°$. (B) Focal line of the modified Bainbridge–Jordan mass spectrograph (with $\varepsilon'' = -49°$). × = direction-focusing point and ◇ = energy-focusing point. A fitted direction-focusing line results in $\kappa = 65.6°$. A fitted energy-focusing results in $\kappa = 65.6°$.

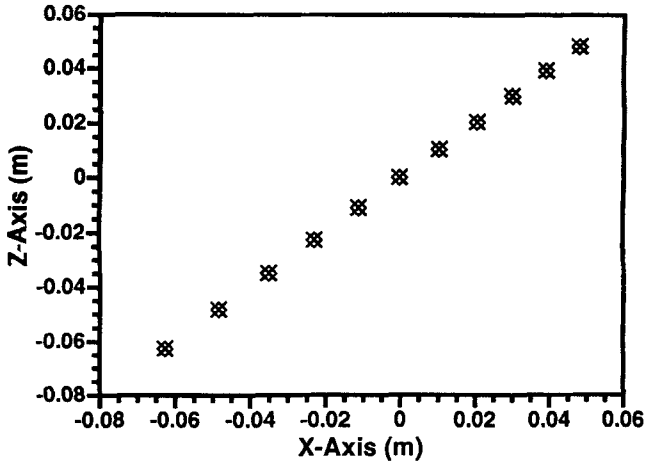

FIGURE 12. Focal line of the Mattauch–Herzog mass spectrograph. × = direction-focusing point and ◇ = energy-focusing point. A fitted direction-focusing line results in $\kappa = 45.0°$. A fitted energy-focusing line results in $\kappa = 45.0°$.

D. Hintenberger–Konig

Hintenberger and Konig calculated 64 mass spectrometer and 65 mass spectrograph double-focusing geometries (Hintenberger & Konig, 1959). In addition, various second-order ion-optic parameters were calculated. We recommend the article to the interested reader. One geometry was chosen at random from among those calculated, and is presented here (Figs. 16 and 17).

E. Takeshita

Takeshita utilized two electric sectors in a "Mattauch-Herzog type" design in order to eliminate some second-

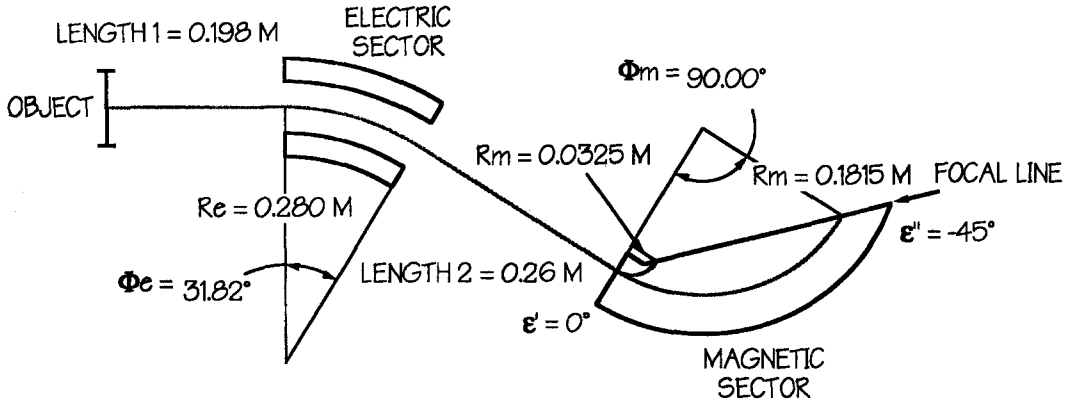

FIGURE 11. Diagram of the Mattach–Herzog mass spectrograph geometry.

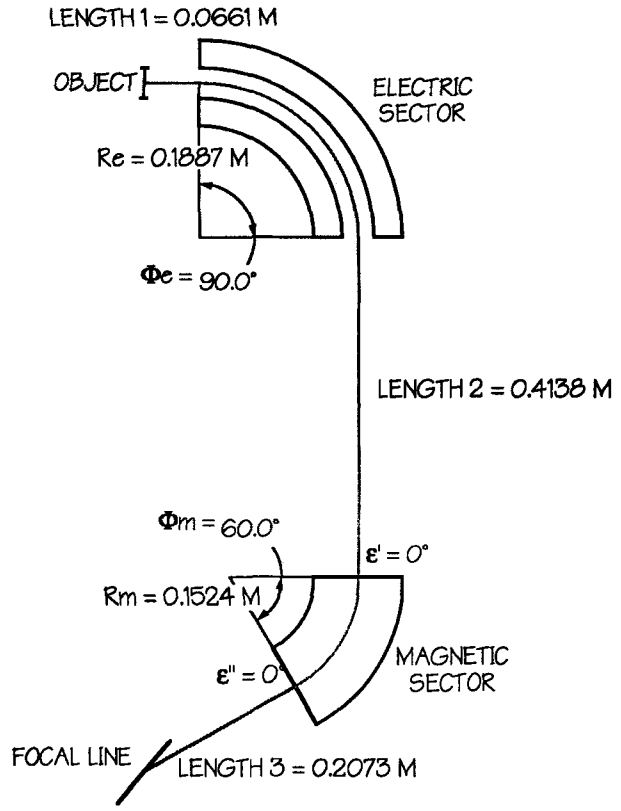

FIGURE 13. Diagram of the Nier–Johnson mass spectrograph geometry.

order aberrations (Fig. 18) (Takeshita, 1967). Two electric sectors are used to independently control the velocity spread of the beam divergence. The calculated direction and energy focal lines overlap well (Fig. 19).

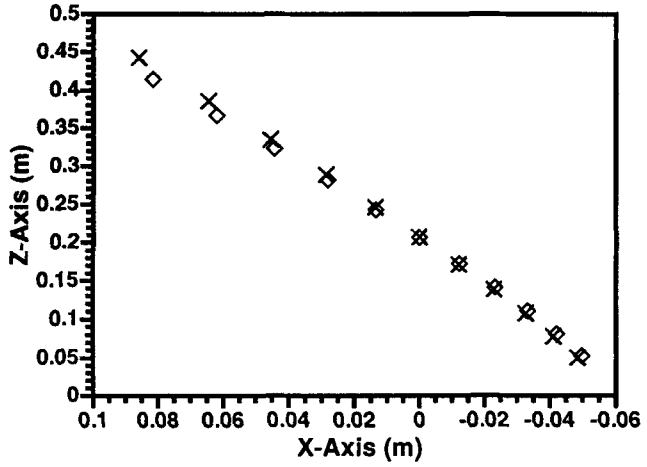

FIGURE 14. Focal line of the Nier–Johnson mass spectrograph. × = direction-focusing point and ◇ = energy-focusing point. A fitted direction-focusing line results in κ = 70.9°. A fitted energy-focusing line results in κ = 69.9°.

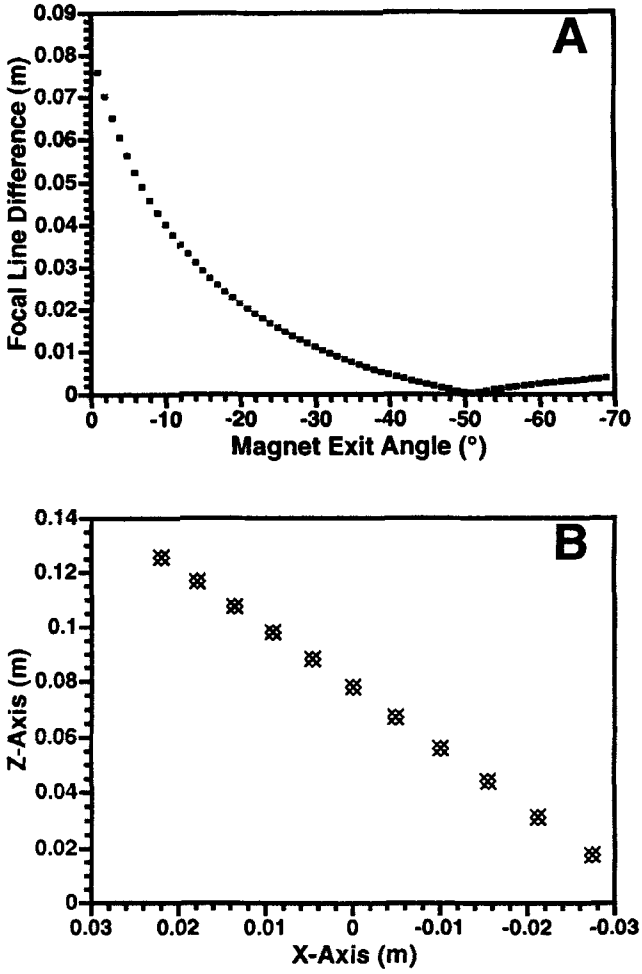

FIGURE 15. (A) Difference in direction and energy focal lines as a function of oblique exit angle of the magnetic sector (ε''). The smallest distance between focal lines is ε'' = −49°. (B) Focal line of the modified Bainbridge–Jordan mass spectrograph (with ε'' = −51°). × = direction-focusing point and ◇ = energy-focusing point. A fitted direction-focusing line results in κ = 65.4°. A fitted energy-focusing results in κ = 65.4°.

F. Matsuda

Matsuda designed a double-focusing mass spectrometer (focusing at one point) that eliminated all second-order aberrations and that included the influence of fringing fields (Fig. 20) (Matsuda, 1974). In this geometry, a quadrupole lens was included between the electric and magnetic sectors to improve the focusing in the y-direction. Though designed as a point-focusing mass spectrometer, focal-line studies reveal a linear focal line (Fig. 21) (Matsuo, Sakurai, & Derrick, 1989). For Fig. 21, the quadrupole voltage was optimized for our initial ion beam configuration.

G. Others

Given the large number of mass spectrographs that have been designed and constructed, only a few instruments

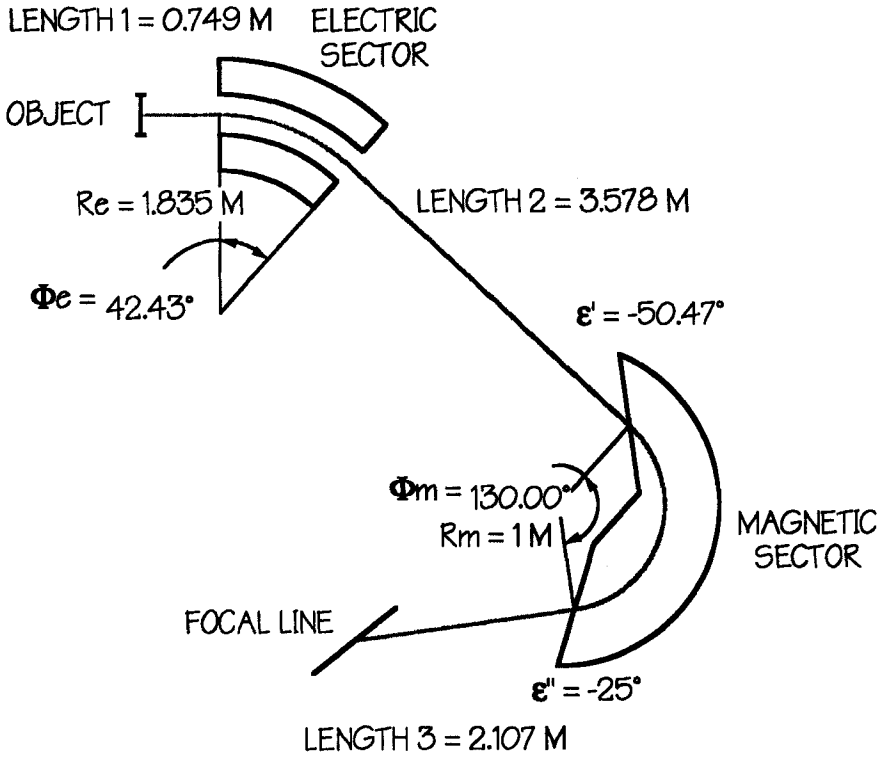

FIGURE 16. Diagram of a Hintenberger–Konig mass spectrograph geometry.

could be discussed above in detail. However, a cross-section of additional mass spectrographs that the authors find interesting are mentioned here. Ishihara and Kammei (1989) and Hill et al. (1991) added a lens system (a quadrupole/octapole/quadrupole combination) to vary the mass range and resolution of a mass spectrograph. This lens system was located between the magnetic sector and focal plane. With this system, one could either have a broad mass range and fit as many masses onto the detector as possible, or have a small number of masses on the detector and increase the resolution of the instrument. Previously, Tuithof and Boerboom (1976) achieved the same variable dispersion with a magnetic-quadrupole, magnetic-sector, and electrostatic-quadrupole combination. A unique mass spectrograph that was built specifically for spacecraft experiments consists of a cylindrically symmetrical electric sector followed by several wedge magnets fanning outward (an "orange"-type mass spectrometer) (Copland, Moore, & Hoffman, 1984; Hirahara & Mukai, 1993). This cylindrical symmetry offers a larger entrance aperture, which can sample a large portion of an extended ion source. Matsuda and Wollnik designed a mass spectrograph consisting of a Wien filter followed by a magnetic sector (Matsuda & Wollick, 1988). A Wien filter (Aberth & Wollnik, 1990; Wien, 1902) is advantageous for analyzing ions of roughly equal velocity over a wide mass range (wide energy spread). This mass spectrograph was designed for the analysis of collision fragments in tandem mass spectrometry. Matsuo and Ishihara designed new

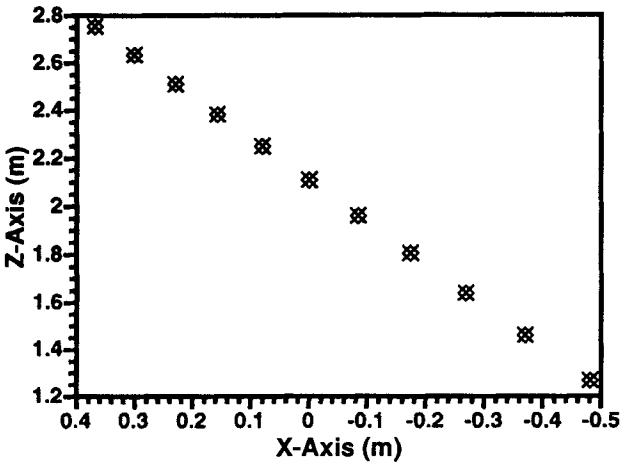

FIGURE 17. Focal line of a Hintenberger–Konig mass spectrograph. × = direction-focusing point and ◇ = energy-focusing point. A fitted direction-focusing line results in $\kappa = 60.2°$. A fitted energy-focusing line results in $\kappa = 60.2°$.

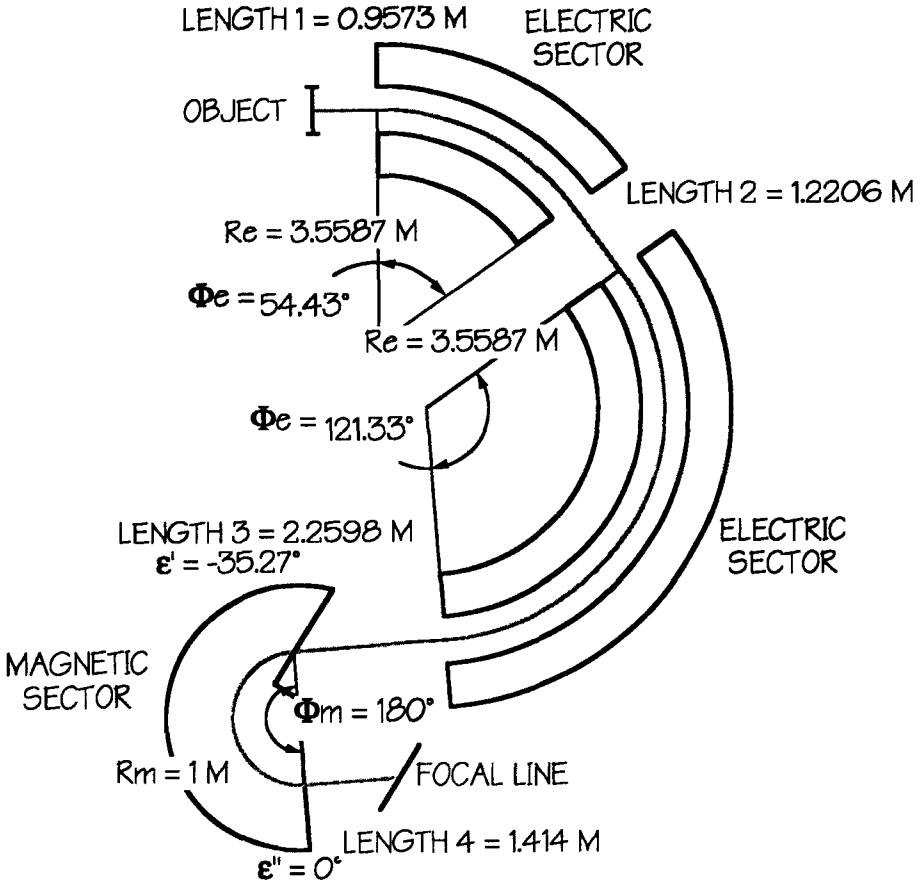

FIGURE 18. Diagram of a Takeshita mass spectrograph geometry.

mass spectrographs based on either a Nier–Johnson or Mattauch–Herzog geometry (Matsuo & Ishihara, 1993). In general, geometries similar to the Mattauch–Herzog mass spectrograph with electrostatic quadrupoles between the two sectors were calculated to offer the best focusing over an extended mass range.

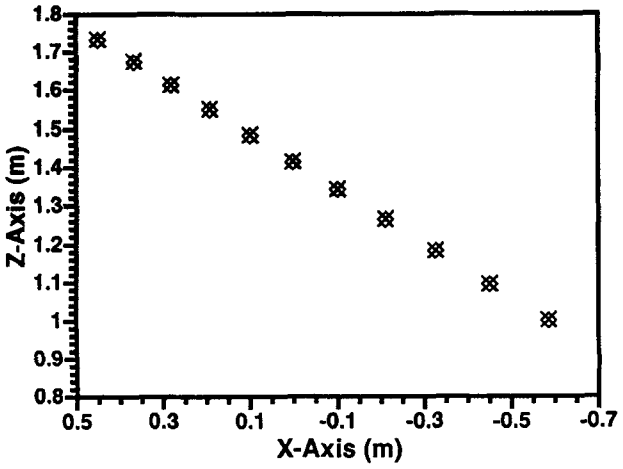

FIGURE 19. Focal line of the Takeshita mass spectrograph. × = direction-focusing point and ◇ = energy-focusing point. A fitted direction-focusing line results in κ = 35.3°. A fitted energy-focusing line results in κ = 35.3°.

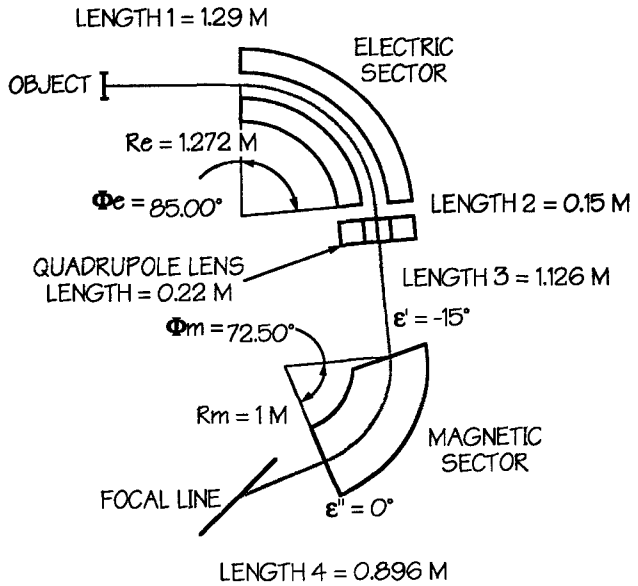

FIGURE 20. Diagram of a Matsuda mass spectrograph geometry.

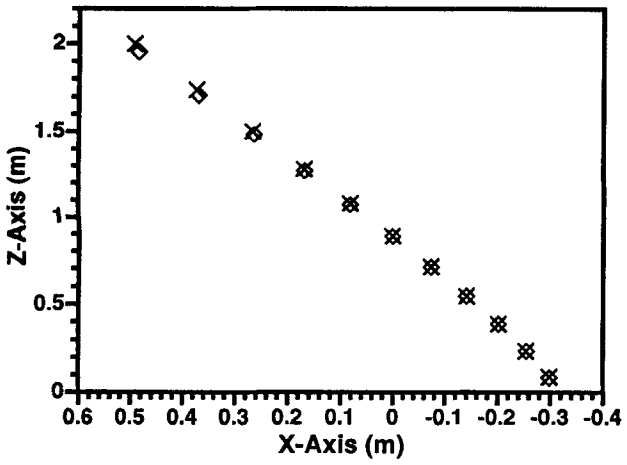

FIGURE 21. Focal line of a Matsuda mass spectrograph. × = direction-focusing point and ◇ = energy-focusing point. A fitted direction-focusing line results in κ = 67.2°. A fitted energy-focusing line results in κ = 66.9°.

IV. CONCLUSIONS

Relatively simple calculations can be used to determine the direction and energy focal-line locations of mass spectrograph geometries. These calculations were limited here to first-order approximations using drift lengths, electrostatic quadrupoles, and electric and magnetic sectors. Mass spectrograph geometries such as those developed by Bainbridge and Jordan, Mattauch and Herzog, and Matsuo were investigated. In some cases, for example, in the Bainbridge–Jordan geometry, a change in the oblique exit of the magnetic sector results in improved overlap of the direction and energy focal lines.

The current weak link in mass spectrograph development is the detector. Its relatively high cost and narrow linear dynamic range are the Achilles heel of these instruments. Nevertheless, mass spectrographs provide excellent sensitivity, the ability to detect transient samples, and exceptional precision and are useful in selected mass spectrometric measurements. Examples of mass spectrograph use could be isotope ratio, laser ablation analysis, and fast gas chromatographic analysis. It is expected that, as array detector technology improves, so too should mass spectrograph development and use.

ACKNOWLEDGEMENTS

This research was supported in part by the National Institutes of Health through grant GM 53560.

REFERENCES

1. Aberth, W.; Wollnik, H. "The Wien filter and its application in chemistry," *Mass Spectrom. Rev.* **1990,** *9,* 383–404.
2. Alexeff, I. "Throughput limit in mass spectrograph-type isotope separators," *J. Appl. Phys.* **1973,** *44,* 4592–4594.
3. Alexeff, I. "Comment on 'A Critique of the Throughput Limit in Mass Spectrographs,'" *J. Appl. Phys.* **1978,** *49,* 5668.
4. Aston, F. W. "A positive ray spectrograph," *Phil. Mag.* **1919,** *38,* 707–714.
5. Aston, F. W. *Mass Spectra and Isotopes;* 2nd ed.; Edward Arnold: London, **1942.**
6. Bainbridge, K. T.; Jordan, E. B. "Mass spectrum analysis 1. The mass spectrograph 2. The existence of isobars of adjacent elements," *Phys. Rev.* **1936,** *50,* 282–296.
7. Bainbridge, K. T. "Charged particle dynamics and optics, relative isotopic abundances of the elements, atomic masses." In *Experimental Nuclear Physics;* Segre, E., Ed.; John Wiley & Sons: New York, **1953,** Vol. 1, pp. 559–766.
8. Bakker, J. M. B. "New mass spectrometer/mass spectrograph," *Int. J. Mass Spectrom. Ion Phys.* **1973,** *11,* 305–307.
9. Banford, A. P. *The Transport of Charged Particle Beams;* E. & F. N. Spon: London, **1966.**
10. Barber, N. F. "Note on the shape of an electron beam bent in a magnetic field," *Proc. Leeds Philos. Soc. Sci. Sect.* **1933,** *2,* 427–434.
11. Berthod, J.; Stefani, R. "Experimental and mathematical determination of the image plane in a spark source mass spectrograph," *Int. J. Mass Spectrom. Ion Phys.* **1976,** *22,* 121–134.
12. Beynon, J. H.; Jones, D. O.; Cooks, R. G. "Imaging detector for mass spectrometry," *Anal. Chem.* **1975,** *47,* 1734–1738.
13. Birkinshaw, K. "Focal plane charge detector for use in mass spectrometry," *Analyst* **1992,** *117,* 1099–1104.
14. Boerboom, A. J. H.; Meuzelar, H. L. C. "Simultaneous detection of large mass spectra using unequally spaced multichannel plates in double exposure," *Int. J. Mass Spectrom. Ion Proc.* **1988,** *86,* 21–29.
15. Boerboom, A. J. H. "Array detection of mass spectra, a comparison with conventional detection methods," *Org. Mass Spectrom.* **1991,** *26,* 929–935.
16. Boettger, H. G.; Giffen, C. E.; Norris, D. D. "Electro-optical ion detectors in mass spectrometry simultaneous monitoring of all ions over wide mass ranges." In *ACS Symposium Series no. 102;* Talmi, Y., Ed.; ACS: Washington, D.C., **1979,** 291–318.
17. Bradshaw, N.; Hall, E. F. H.; Sanderson, N. E. "Inductively coupled plasma as an ion source for high resolution mass spectrometry," *J. Anal. At. Spectrom.* **1989,** *4,* 801–803.
18. Bratschi, O.; Ghielmetti, A. G.; Shelley, E. G.; Balsiger, H. "Experimental tests of a mass-angle spectrograph with poloidal ion optics," *Rev. Sci. Instrum.* **1993,** *64,* 184.
19. Brown, K. L.; Belbeoch, R.; Bounin, P. "First- and second-order magnetic optics matrix equations for the midplane

of uniform-field wedge magnets," *Rev. Sci. Instrum.* **1964,** *35,* 481–485.

20. Burgoyne, T. W. Ph. D. thesis, "An atmospheric endosulfan investigation and the development of a plasma-source mass spectrograph," Indiana University, Bloomington, **1996.**
21. Burgoyne, T. W.; Hieftje, G. M.; Hites, R. A. "The design and performance of a plasma source mass spectrograph," *J. Am. Soc. Mass Spectrom.* **1996,** to appear.
22. Burlingame, A. L.; Walls, F. C.; Falick, A.; Evans, S.; Buchanan, R. "Experience in the use of a 4-sector instrument and array detector and its application in peptide analysis," *Rapid Commun. Mass Spectrom.* **1990,** *4,* 447–448.
23. Carrico, J. P.; Johnson, M. S.; Somer, T. A. "Postion sensitive charged particle detector for a miniature Mattauch–Herzog mass spectrometer," *Int. J. Mass Spectrom. Ion Phys.* **1973,** *11,* 409–415.
24. Chamel, A.; Eloy, J. F. "Microanalysis with the laser probe mass spectrograph (LPMS) in plant biology," *J. Phys., Colloq.* **1984,** 573–576.
25. Cody, R. B.; Tamura, J.; Finch, J. W.; Musselman, B. D. "Improved detection limits for electrospray ionization on a magnetic sector mass spectrometer using an array detector," *J. Am. Soc. Mass Spectrom.* **1994,** *5,* 194–200.
26. Coplan, M. A.; Moore, J. H.; Hoffman, R. A. "Double focusing ion mass spectrometer of cylindrical symmetry," *Rev. Sci. Instrum.* **1984,** *55,* 537–541.
27. Cottrell, J. S.; Evans, S. "The application of a multichannel electro-optical detection system to the analysis of large molecules by FAB mass spectrometery," *Rapid Commun. Mass Spectrom.* **1987,** *1,* 1.
28. Cottrell, J. S.; Evans, S. "Characteristics of a multichannel electrooptical detection system and its application to the analysis of large molecules by fast atom bombardment mass spectrometry," *Anal. Chem.* **1987,** *59,* 1990–1995.
29. Courant, E. D.; Livingston, M. S.; Snyder, H. S. "The strong-focusing synchroton—A new high energy accelerator," *Phys. Rev.* **1952,** *88,* 1190–1196.
30. Cromwell, E. F.; Arrowsmith, P. "Novel multichannel plasma-source mass spectrometer," *J. Am. Soc. Mass Spectrom.* **1996,** *7,* 458–466.
31. Dahl, P. *Introduction to Electron and Ion Physics;* Academic Press: New York, **1973.**
32. Dawson, P. H. *Quadrupole Mass Spectrometry and its Applications;* American Institute of Physics: New York, **1995.**
33. Dempster, A. J. "New methods in mass spectrometry," *Proceedings of the American Philosophical Society,* **1935,** *75,* 755–767.
34. Dempster, A. J. "A new method of positive ray analysis," *Phys. Rev.* **1918,** *11,* 316–325.
35. Denison, D. R. "Operating parameters of a quadrupole in a grounded cylindrical housing," *J. Vacuum Sci. Tech.* **1971,** *8,* 266–269.
36. Donohue, D. L.; Carter, J. A.; Mamantov, G. "An electro-optical ion detector for spark source mass spectrometry," *Int. J. Mass Spectrom. Ion Phys.* **1980,** *33,* 45–55.
37. Dreyer, W. J.; Kuppermann, A.; Boettger, H. G.; Giffin, C. E.; Norris, D. D.; Grotch, S. L.; Theard, L. P. "Automatic mass-spectrometric analysis. Preliminary report on development of a novel mass-spectrometric system for biomedical applications," *Clin. Chem.* **1974,** *20,* 998–1002.
38. Enge, H. A. "Magnetic spectrographs," *Physics Today* **1967,** *20,* 65–75.
39. Enge, H. A. "Deflecting magnets." In *Focusing of Charged Particles;* Septier, A., Ed.; Academic Press: New York, **1967,** Vol. 2, pp. 203–264.
40. Enge, H. A. "Particle detection systems," *IEEE Trans. Nucl. Sci.* **1979,** *NS26,* 2420–2426.
41. Enge, H. A.; Betz, H. D.; Buechner, W. W.; Grodzins, L.; Moore, W. H.; Kanter, E. P. "Proposed recoil mass spectrograph for detecting superheavy nuclei," *Nucl. Instrum. Methods* **1971,** *97,* 449–457.
42. Enge, H. A.; Horn, D. "Performance of an energy-mass spectrograph for heavy ions," *Nucl. Instrum. Methods* **1977,** *145,* 271–277.
43. Ewald, H.; Sauermann, G.; Liebl, H. "The performance and image error correction of the new stigmatic focusing mass spectrograph." In *Advances in Mass Spectrometry;* Waldron, J. D., Ed.; Pergamon Press: New York, **1959,** Vol. 1, pp. 10–15.
44. Forrester, A. T.; Perel, J.; Mahoney, J. "A critique of the throughput limit in mass spectrographs," *J. Appl. Phys.* **1978,** *49,* 3046–3048.
45. Furuta, N. "Optimization of the mass scanning rate for the determination of lead isotopes using an inductively coupled plasma mass spectrometer," *J. Anal. At. Spectrom.* **1991,** *6,* 199.
46. Ghielmetti, A. G.; Shelley, E. G.; Fuselier, S. A.; Herrero, F.; Smith, M. F.; Wurz, P.; Bochsler, P.; Stephen, T. "Mass spectrograph for imaging low energy neutral atoms," *Opt. Eng.* **1993,** *33,* 362–370.
47. Ghielmetti, A. G.; Young, D. T. "A double-focusing toroidal mass spectrograph for energetic plasmas. I. First-order theory," *Nucl. Instrum. Methods Phys. Res.* **1987,** *A258,* 297–303.
48. Giffen, C. E.; Boettger, H. G.; Norris, D. D. "An electro-optical detector for focal plane mass spectrometers," *Int. J. Mass Spectrom. Ion Phys.* **1974,** *15,* 437–449.
49. Gross, M. L. "Tandem mass spectrometry: Multisector magnetic instruments." In *Methods in Enzymology: Mass Spectrometry;* McCloskey, J. A., Ed.; Academic Press: San Diego, **1990,** Vol. 193, pp. 131–153.
50. Gross, M. L.; Cerny, R. L.; Giblin, D. E.; Rempel, D. L.; MacMillan, D. K.; Hu, P.; Holliman, C. L. "Mass spectrometric methods: An answer for macromolecular analysis in the 1990's," *Anal. Chim. Acta* **1991,** *250,* 105–130.
51. Hayes, J. M. "Resolution and sensitivity in organic chemical mass spectrography," *Anal. Chem.* **1969,** *41,* 1966–1973.
52. Hedfjall, B.; Ryhage, R. "Electo-optical ion detector for capillary column gas chromatography/negative ion mass spectrometry," *Anal. Chem.* **1979,** *51,* 1687–1690.

53. Hedfjall, B.; Ryhage, R. "Electrooptical ion detector for gas chromatography/mass spectrometry," *Anal. Chem.* **1981,** *53,* 1641–1644.
54. Hedin, A. E.; Nier, A. O. "A determination of the neutral composition, number density, and temperature of the upper atmosphere from 120 to 200 kilometers with rocket-borne mass spectrometers," *J. Geophys. Res.* **1966,** *71,* 4121–4131.
55. Herzog, R. F. K. "Neue Erkenntnisse uber die Elektronenoptischen Eigenschaften Magnetischer Ablenkfelder," *Acta Physica Austriaca* **1950,** *4,* 431–444.
56. Herzog, R.; Hauk, V. "Electronenoptische Theorie der derzeit in Verwendung stehenden Prazisionsmassenspektrographen," *Z. Physik* **1938,** *108,* 609–634.
57. Hill, J. A.; Biller, J. E.; Martin, S. A.; Biemann, K.; Yoshidome, K.; Sato, K. "Design considerations, calibration and applications of an array detector for a four sector tandem mass spectrometer," *Int. J. Mass Spectrom. Ion Proc.* **1989,** *92,* 211–230.
58. Hill, J. A.; Biller, J. E.; Biemann, K. "A variable dispersion array detector for a tandem mass spectrometer," *Int. J. Mass Spectrom. Ion Proc.* **1991,** *111,* 1–25.
59. Hintenberger, H.; Konig, L. A. "Mass spectrometers and mass spectrographs corrected for image defects." In *Advances in Mass Spectrometry;* Waldron, J. D., Ed.; Pergamon Press: New York, **1959,** Vol. 1, pp 16–35.
60. Hirahara, M.; Mukai, T. "Satellite borne energetic mass spectrometer for three dimensional measurement of velocity distribution," *Rev. Sci. Instrum.* **1993,** *64,* 406–419.
61. Hughes, A. L.; Rojansky, V. "On the analysis of electronic velocities by electrostatic means," *Phys. Rev.* **1929,** *34,* 284–290.
62. Ioanoviciu, D. "Ion Optics." In *Advances in Electronics and Electron Physics;* Hawkes, P. W., Ed.; Academic Press: Boston, **1989,** Vol. 73, pp. 1–92.
63. Ishihara, M.; Kammei, Y. "Ion optical considerations of a quadrupole-octapole lens system for varying mass range on a simultaneous detector," *Rapid Commun. Mass Spectrom.* **1989,** *3,* 420–423.
64. JEOL; http://www.jeol.com/ms/ccdarray.html, **1996.**
65. Johnson, E. G. N., A. O. "Angular aberrations in sector shaped electromagnetic lenses for focusing beams of charged particles," *Phys. Rev.* **1953,** *91,* 10–17.
66. Jordan, E. B. "The mass differences of the fundamental doublets used in the determination of the isotopic weights C12 and N14," *Phys. Rev.* **1941,** *60,* 710–713.
67. Leclercq, P. A.; Cramers, C. A. "GC/MS and the chromatographic challenge," *J. High Res. Chrom. and Chrom. Comm.* **1988,** *11,* 845–848.
68. Leclercq, P. A.; Snijders, H. M. J.; Cramers, C. A.; Maurer, K. H.; Rapp, U. "Rapid and ultrasensitive GC/MS analysis with a microchannel plate array detector, Part I. Possibilities of simultaneous ion detection in narrow bore GC/MS," *J. High Res. Chrom.* **1989,** *12,* 652–656.
69. Li, G.; Duhr, A.; Wollnik, H. "A new tandem mass spectrometer for the study of molecular dissociations," *J. Am. Soc. Mass Spectrom.* **1992,** *3,* 487–492.
70. Louter, G. J.; Boerboom, A. J. H.; Stalmeier, P. F. M.; Tuithof, H. H.; Kistemaker, J. "A tandem mass spectrometer for collision-induced dissociation," *Int. J. Mass Spectrom. Ion Phys.* **1980,** *33,* 335–347.
71. Louter, G. J.; Buijserd, A. N. "A very sensitive electro-optical simultaneous ion detection system," *Int. J. Mass Spectrom. Ion Phys.* **1983,** *50,* 245–257.
72. Louter, G. J.; Buijserd, A. N.; Boerboom, A. J. H. "A very sensitive electro-optical simultaneous ion detection system," *Int. J. Mass Spectrom. Ion Phys.* **1983,** *46,* 131–134.
73. Mai, H.; Wagner, H. "Design for improvement of sensitivity of mass spectrographs," *J. Sci. Instrum.* **1967,** *44,* 883–885.
74. Mantus, D. S.; Valaskovic, G. A.; Morrison, G. H. "High mass resolution secondary ion mass spectrometry via simultaneous detection with a charge-coupled device," *Anal. Chem.* **1991,** *63,* 788–792.
75. Matsuda, H. "Double focusing mass spectrometers of second order," *Int. J. Mass Spectrom. Ion Phys.* **1974,** *14,* 219–233.
76. Matsuda, H. "High-resolution high-sensitivity mass spectrometers," *Mass Spectrom. Rev.* **1983,** *2,* 299–325.
77. Matsuda, H. "A new mass spectrograph for the analysis of dissociation fragments," *Int. J. Mass Spectrom. Ion Proc.* **1989,** *91,* 11–17.
78. Matsuda, H.; Wollnik, H. "A mass spectrograph for the analysis of collisionally activated molecular fragments," *Int. J. Mass Spectrom. Ion Proc.* **1988,** *86,* 53–59.
79. Matsuda, H.; Wollnik, H. "Second-order double-focusing mass spectrograph with a wide mass range," *Int. J. Mass Spectrom. Ion Proc.* **1989,** *91,* 19–26.
80. Matsuo, T.; Ishihara, M. "A new mass spectrograph," *J. Am. Soc. Mass Spectrom.* **1993,** *4,* 372–386.
81. Matsuo, T.; Matsuda, H.; Fujita, Y.; Wollnik, H. "Computer program TRIO for third-order calculation of ion trajectory," *Mass Spectrosc.* **1976,** *24,* 19–61.
82. Matsuo, T.; Sakurai, T.; Derrick, P. "Characterization of the focal planes of a mass spectrometer using the method of transfer matrixes," *Int. J. Mass Spectrom. Ion Proc.* **1989,** *91,* 41–49.
83. Matsuo, T.; Sakurai, T.; Ishihara, M. "Recent developments of ion-optical studies for mass spectrometer and mass spectrograph design," *Nucl. Instrum. Meth.* **1990,** *A298,* 134–141.
84. Mattauch, J. "Precision mass spectroscopy and theory of dispersion." In *Mass Spectroscopy in Physics Research;* Hipple, J. A., Ed.; National Bureau of Standards: Washington, **1953,** Circular 522, pp 1–27.
85. Mattauch, J.; Herzog, R. "Uber Einen Neuen Massenspectrographen," *Z. Physik* **1934,** *89,* 786–795.
86. Mattauch, J. "A double focusing mass spectrograph and the masses of N15 and O18," *Phys. Rev.* **1936,** *50,* 617–623.

87. Mauersberger, K. "Mass spectrometer beam system for applications in the stratosphere," *Rev. Sci. Instrum.* **1977,** *48,* 1169–1173.

88. Mauersberger, K.; Finstad, R. "Further laboratory studies and stratospheric flight of a mass spectrometer beam system," *Rev. Sci. Instrum.* **1979,** *50,* 1612–1617.

89. McDowell, C. *Mass Spectrometry;* McGraw-Hill: New York, **1963.**

90. Moore, J. H.; Davis, C. C.; Coplan, M. A. "Charged-particle optics." In *Building Scientific Apparatus: A Practical Guide to Design and Construction;* Addison–Wesley: Redwood City, **1983,** 287–325.

91. Moore, T. E. "Spectrograph suitable for the mass and energy analysis of space plasmas over the energy range 0.1–10 keV," *Rev. Sci. Instrum.* **1977,** *48,* 221–225.

92. Murphy, D. M.; Mauersberger, K. "Operation of a microchannel plate counting system in a mass spectrometer," *Rev. Sci. Instrum.* **1985,** *56,* 220–226.

93. Murphy, D. M.; Mauersberger, K. "A highly sensitive mass spectrometer detector system," *Int. J. Mass Spectrom. Ion Proc.* **1987,** *76,* 85–93.

94. Nier, A. O.; Hayden, J. L. "A miniature Mattauch–Herzog mass spectrometer for the investigation of planetary atmospheres," *Int. J. Mass Spectrom. Ion Phys.* **1971,** *6,* 339–346.

95. Nier, A. O.; Potter, W. E.; Hickman, D. R.; Mauersberger, K. "The open-source neutral-mass spectrometer on atmosphere explorer-C, -D, and -E," *Radio Science* **1973,** *8,* 271–276.

96. Nier, A. O.; Roberts, T. R. "The determination of atomic mass doublets by means of a mass spectrometer," *Phys. Rev.* **1951,** *81,* 507–510.

97. Nier, A. O.; Schlutter, D. J. "High performance double focusing mass spectrometer," *Rev. Sci. Instrum.* **1985,** *56,* 214–219.

98. Nowak, P. J. C. M.; Holsboer, H. H.; Heubers, W.; Wijnaendts van Resandt, R. W.; Los, J. "A parallel detection system for a mass spectrometer," *Int. J. Mass Spectrom. Ion Phys.* **1980,** *34,* 375–382.

99. Ogata, K.; Matsuda, H. "Masses of light atoms," *Phys. Rev.* **1953,** *89,* 27–32.

100. Oron, M. "A static field mass spectrograph for laser induced plasma experiments," *Nucl. Instrum. Methods* **1976,** *139,* 235–237.

101. Oron, M.; Paiss, Y. "A dynamic mass spectrometer for the study of laser produced plasmas," *Rev. Sci. Instrum.* **1973,** *44,* 1293–1296.

102. Penner, S. "Calculations of properties of magnetic deflection systems," *Rev. Sci. Instrum.* **1961,** *32,* 150–160.

103. Rytz, C.; Kopp, E.; Eberhardt, P. "Simultaneous ion detection mass spectrometer for the measurement of stratospheric trace gases," *Int. J. Mass Spectrom. Ion Proc.* **1994,** *137,* 55–66.

104. Salomaa, M.; Enge, H. A. "Velocity selector for heavy-ion separation," *Nucl. Instrum. Meth.* **1977,** *145,* 279–282.

105. Sinha, M. P. "Characterization of individual particles in gaseous media by mass spectrometry." In *Particles in Gases and Liquids 2;* Mitfal, K., Ed.; Plenum Press: New York, **1990,** 197–209.

106. Sinha, M. P.; Gutnikov, G. "Development of a minaturized gas chromatograph-mass spectrometer with a microbore capillary column and an array detector," *Anal. Chem.* **1991,** *63,* 2012–2016.

107. Sinha, M. P.; Gutnikov, G. "Role of a microbore capillary column in the development of a portable gas chromatograph-mass spectrometer," *J. Microcolumn Sep.* **1992,** *4,* 405–410.

108. Sinha, M. P.; Tomassian, A. D. "Development of a miniaturized, light weight magnetic sector for a field portable mass spectrograph," *Rev. Sci. Instrum.* **1992,** *62,* 2618–2620.

109. Spencer, N. W.; Reber, C. A. "A mass spectrometer for an aeronomy satellite," *Space Res.* **1963,** *3,* 1151–1155.

110. Staub, H. H. "Detection methods," In *Experimental Nuclear Physics;* Segre, E., Ed.; John Wiley and Sons: New York, **1953,** Vol. 1, pp 64–71.

111. Takeshita, I. "Mattauch–Herzog type mass spectrograph with corrected .beta.-dependent image defects for all masses," *Rev. Sci. Instrum.* **1967,** *38,* 1361–1367.

112. Taylor, S. R.; Gorton, M. P. "Geochemical application of spark source mass spectrography. III. Element sensitivity, precision and accuracy," *Geochim. Cosmochim. Acta* **1977,** *41,* 1375–1380.

113. Thomson, J. J. *Rays of Positive Electricity and their Application to Chemical Analyses;* Longmans Green: London, **1913.**

114. Thomson, J. J.; Thomson, G. P. *Conduction of Electricity Through Gases;* 3rd ed.; Vol. 1; University Press: Cambridge, **1928.**

115. Todd, J. F. J. "Recommendations for nomenclature and symbolism for mass spectrometry," *Int. J. Mass Spectrom. Ion Processes* **1991,** *142,* 211–240.

116. Tsoupas, N.; Cosman, E.; Sperduto, A.; Young, G.; Enge, H.; Salomaa, M. "In-flight mass separation of radon-205, -206, and -207 fusion recoils from the 197Au(14N, xn) reaction using an energy-mass spectrograph," *Nucl. Instrum. Methods* **1978,** *148,* 93–97.

117. Tuithof, H. H.; Boerboom, J. H.; Meuzelaar, H. L. "Simultaneous detection of a mass spectrum using a channeltron electron multiplier array," *Int. J. Mass Spectrom. Ion Phys.* **1975,** *17,* 299–307.

118. Tuithof, H. H. B., J. H. "Variation of the dispersion, resolution and inclination of the focal plane of a single-focusing mass spectrometer by use of two quadrupoles," *Int. J. Mass Spectrom. Ion Phys.* **1976,** *20,* 107–121.

119. United States National Bureau of Standards, "Mass spectroscopy in physics research," *Proceedings of the NBS Semicentennial Symposium on Mass Spectroscopy in Physics Research;* NBS Circular 522; Washington, **1953.**

120. von Zahn, U.; Mauersberger, K. "Small mass spectrometer

with extended measurement capabilities at high pressures," *Rev. Sci. Instrum.* **1978,** *49,* 1539–1542.

121. Waegli, P. "Wide energy range mass spectrograph," *Rev. Sci. Instrum.* **1979,** *50,* 165–170.
122. Walder, A. J.; Abell, I. D.; Platzner, I.; Freedman, P. A. "Lead isotope ratio measurement of NIST 610 glass by laser ablation inductively coupled plasma mass spectrometry," *Spectrochim. Acta* **1993,** *48B,* 397–402.
123. Walder, A. J.; Freedman, P. A. "Isotope ratio measurement using a double focusing magnetic sector mass analyzer with an inductively coupled plasma as an ion source," *J. Anal. At. Spectrom.* **1992,** *7,* 571–575.
124. Walder, A. J.; Platzner, I.; Freedman, P. A. "Isotope ratio measurement of lead, neodymium and newdymium-samarium mixtures, hafnium-lutetium mixtures with a double focusing multiple collector inductively coupled plasma mass spectrometer," *J. Anal. At. Spectrom.* **1993,** *8,* 19–23.
125. Wien, W. "Untersuchungen uber die Elektrische Entladung in Verdunnten Gasen," *Annalen der Physik* **1902,** *8,* 244–266.
126. Wirsz, D. F.; Browne, R. J.; Blades, M. W. "Dynamic range enhancement of photodiode array spectra," *Appl. Spectrosc.* **1987,** *41,* 1383–1387.
127. Wiza, J. L. "Microchannel Plate Detectors," *Nucl. Instrum. Meth.* **1979,** *162,* 587–601.
128. Wollnik, H. "Image aberrations of second order for magnetic and electrostatic sector fields including all fringing field effects," *Nucl. Instrum. Meth.* **1965,** *38,* 56–58.
129. Wollnik, H. "Second order transfer matrices of real magnetic and electrostatic sector fields," *Nucl. Instrum. Meth.* **1967,** *52,* 250–272.
130. Wollnik, H. "Electrostatic prisms." In *Focusing of Charged Particles;* Septier, A., Ed.; Academic Press: New York, **1967,** Vol. 2, pp. 163–202.
131. Wollnik, H. "Mass spectrographs and isotope separators," In *Advances in Electronics and Electron Physics;* Septier, A., Ed.; Academic Press: New York, **1980,** Vol. 13B, pp. 133–172.
132. Wollnik, H. *Optics of Charged Particles;* Academic Press: San Diego, **1987.**
133. Wollnik, H.; Brezina, J.; Wendel, W. "GIOS-Beamtrace, a program for the design of high resolution mass spectrometers," *Atomic Masses and Fundamental Constants: Proceedings of the 7th International Conference on Atomic Masses and Fundamental Constants,* Darmstadt–Seeheim, September 3–7, **1984,** Technische Hochschule Darmstadt; 679–683.
134. Wollnik, H.; Brezina, J.; Berz, M. "GIOS-Beamtrace—A program package to determine optical properties of intense ion beams," *Nucl. Instrum. Meth.* **1987,** *A258,* 408–411.
135. Wollnik, H.; Ewald, H. "The influence of magnetic and electric fringing fields on the trajectories of charged particles," *Nucl. Instrum. Meth.* **1965,** *36,* 93–104.
136. Wurz, P.; Aellig, M. R.; Bochsler, P.; Ghielmetti, A. G.; Shelley, E. G.; Fuselier, S. A.; Herrero, F.; Smith, M. F.; Stephen, T. "Neutral atom imaging mass spectrograph," *Opt. Eng.* **1995,** *34,* 2365–2376.
137. Yavor, M. I. "Methods for calculation of parasitic aberrations and machining tolerances in electron optical systems." In *Advances in Electronics and Electron Physics;* Hawkes, P. W., Ed.; Academic Press: Boston, **1993,** Vol. 86, pp. 225–281.
138. Young, D. T.; Marshall, J. A.; Burch, J. L.; Booker, T. L.; Ghielmetti, A. G.; Shelley, E. G. "A double-focusing toroidal mass spectrograph for energetic plasmas. II. Experimental results," *Nucl. Instrum. Methods Phys. Res.* **1987,** *A258,* 304–309.